Three-dimensional time-varying large surface displacements in coal exploiting areas revealed through integration of SAR pixel offset measurements and mining subsidence model

Bingqian Chen[a,b,c,d], Zhenhong Li[b,c,*], Chen Yu[b], David Fairbairn[b], Jianrong Kang[a], Jinshan Hu[a], Liang Liang[a]

[a] School of Geography and Geomatics and Urban-Rural Planning, Jiangsu Normal University, Xuzhou 221116, China
[b] School of Engineering, Newcastle University, Newcastle upon Tyne NE1 7RU, UK
[c] College of Geological Engineering and Geomatics, Chang'an University, Xi'an 710054, China
[d] Hunan Province Key Laboratory of Coal Resources Clean-utilization and Mine Environment Protection, Xiangtan 411201, China

ABSTRACT

Underground mining activities usually induce large surface displacements thus causing serious safety hazards and potential ecological damage. The capability of conventional Interferometric Synthetic Aperture Radar (InSAR) to monitor tectonic movements, volcanic eruptions and city subsidence has been fully demonstrated, but its application to mining subsidence is limited because of the failure caused by localized surface displacements with strong spatial gradients. In this paper, a new method is presented to utilize SAR pixel Offset Tracking (OT) with a single pair of SAR images to resolve three-dimensional (3D) large surface displacements caused by underground coal mining. Coal mining subsidence theory is utilised to analytically separate the vertical and horizontal components. This method is applied to the Daliuta coal mining area in Shaanxi Province, China, where a dense GPS network is available. Results show the RMS differences of OT derived displacements against GPS in both horizontal and vertical directions are in the sub-centimeter level. In addition, a prediction of mining-induced ground movements is performed with the Support Vector Regression algorithm and RMS differences of 12.4, 13.1 and 14.4 cm are observed compared to GPS, in the vertical, easting and northing directions respectively. The framework demonstrated in this paper is not only able to derive the evolution of the 3D large surface displacements with multi-temporal SAR images in a single-geometry, but also has a potential for short-term predication, which can provide early warnings and promote strategic decision-making for engineering management in the process of coal mining.

1. Introduction

Coal provides important energy support for the development of national economy and it is also one of the non-renewable energy sources on the Earth. Intense underground coal mining over a large area leads to serious problems of ground subsidence and potential environmental catastrophe. It was reported that in China the total ground subsidence area as a result of coal mining exceeded 700,000 ha during the period from 1949 to 2002, and the consequent economic loss exceeded 50 billion RMB (equivalent to 7 billon USD) (Li, 2006). On average, the ground subsidence in North and East China exceeded approximately 7000 ha per year. To reduce the catastrophe due to coal-mining-induced ground subsidence, a substantial number of previous studies have been carried out to monitor, characterise and even predict mining subsidence (Guo et al., 2014, 2016; Howladar and Hasan, 2014; Li, 2006; Nie et al., 2015; Salmi et al., 2017; Song et al., 2012; Zhou et al., 2015). Due to the complexity of mining geology and its three-dimensional (3D) nature, previous studies on coal-mining-induced subsidence are primarily based on ground measurements in the field. Traditional monitoring techniques of coal mining subsidence mainly consist of triangulation, levelling and GPS. But these methods have inherent limitations, including point measurements only, large workforce requirements, and cost inefficiency.

Spaceborne repeat-pass Interferometric Synthetic Aperture Radar (InSAR) can achieve sub-centimeter precision and measure large areas (e.g.100 × 100 km² or even wider) with a horizontal spatial resolution of 1–10s meters (e.g. Massonnet and Feigl, 1998). One crucial drawback of InSAR techniques is their incapacity to detect large surface

---

displacements with high spatial gradients (Massonnet et al., 1993; Zebker and Villasenor, 1992). However, coal mining often results in large surface displacements within a very small range and the gradient of the surface displacements can go beyond the maximum detectable deformation gradient of InSAR. Another crucial drawback of InSAR is their incapacity to derive 3D surface displacements from one single orbit imaging geometry. Only the displacement in the radar line of sight (LOS) can be provided by conventional InSAR, which may make interpretation difficult in some cases.

The range offset map from synthetic aperture radar (SAR) pixel Offset Tracking (OT) contains similar LOS range change information to a differential interferogram. Compared with interferometric phase measurements, OT is based on the amplitude information of SAR data and has relatively lower accuracy, typically on the order of 1/20 pixel (Casu et al., 2011). However, OT has the advantages of less vulnerability to temporal and spatial decorrelation effects, greater capacity to measure large deformation and easier access to two-dimensional surface displacements (Michel et al., 1999). OT has been successfully applied to the monitoring of ground motion caused by glaciers, earthquakes, volcanoes, and landslides (Sánchez-Gámez and Navarro, 2017; Li et al., 2011; Singleton et al., 2014). As for deformation monitoring of mining areas, Zhao et al. (2013) was the first to use OT to monitor mining subsidence with a precision of about 1/25 pixel (about 0.2 m). Huang et al. (2016) used OT to map the surface displacements in the mining areas in Daliuta, Shaanxi Province, China. Most previous research efforts using OT to monitor mining subsidence focused on vertical displacements and neglected horizontal movements. There have been limited previous studies working on 3D large mining subsidence. Fan et al. (2015) estimated the extent of 3D surface displacements in the Daliuta mining area by combining OT with a probability integral model (PIM). However, the vertical displacements were retrieved under the assumption that there was no horizontal movement; in addition, they only considered the total ground movements after the coal exploitation finished. Mining subsidence is actually a complex process that evolves in space and time, and it would be optimal to monitor 3D ground displacements and their evolution in time. For a given geology and mining condition, the maximum possible ground subsidence value may occur after the coal exploitation, which is generally located in the centre of subsidence basin. If the size of working panel continues to increase even after the occurrence of the maximum possible value, the width and length of the ground subsidence would increase but the maximum possible subsidence value at the subsidence basin centre would remain unchanged, resulting in a flat bottom at the ground subsidence basin centre and suggesting limited (if any) horizontal movements; this is often defined as supercritical subsidence (e.g. Reddish and Whittaker, 2012). However, the buildings within the supercritical subsidence area can still suffer from deformation or damage because every point in the area is affected when the working panel is advancing. Although such dynamic movement is temporary, it can still lead to damage to buildings. Therefore, it is important to investigate the evolution of dynamic ground movements, assisting in identification of buildings which are influenced by mining activities, and how they evolve at different stages during mining; thus proper protection strategies can be applied to minimise the negative impacts.

Yang et al. (2018) proposed to use OT with the assistance of *a prior* deformation model to derive 3D displacement time-series in a coal mining area. However, 3D surface displacement time-series cannot be fully retrieved using this method for the following reasons. Firstly, the horizontal movements were assumed to be proportional to the tilts, but that assumption does not always hold true (Barbato et al., 2016; He, 1985; He and Ma, 1985; Wu et al., 1998). Secondly, it was assumed that the deformation was linear between two time-adjacent SAR acquisitions, thereby allowing the retrieval of three-dimensional displacements (i.e. vertical, easting, and northing). That assumption is not applicable for coal mining subsidence, as characteristic features of large deformation caused by coal mining can exhibit spatial discontinuity

and temporal non-linearity; Thirdly, the model parameters, including the tangent of the major influential angle and the coefficient of horizontal movements, were considered to be constants in the modelling process, but these parameters should not be fixed when taking into account the nature of the actual movements.

A novel method is presented in this paper to obtain 3D large surface displacements and their evolution in time for coal mining, using multiple SAR images from a single imaging geometry. A distinctive advantage of this new approach is that large 3D ground movements can be accurately resolved from two SAR amplitude images in an identical imaging geometry, i.e. both in ascending orbits and in descending orbits. In this paper, we also attempt to investigate the feasibility to predict mining-induced ground movements using the 3D surface displacements derived from SAR images with a single imaging geometry.

2. Methodology

Different underground mining methods are adopted to extract different minerals under different geological mining conditions. Longwall mining is one of the most commonly used methods, which is a form of underground mining where a long face or wall of minerals is mined in a single slice. Longwall mining is often employed to extract large rectangular blocks of coal, which can be formed using a coal mining machine. The principal idea of longwall mining is to use the support equipment to provide a safe working space for the miners in the mining direction while all the coal seams in the working panel are extracted, and then the supports are removed to allow the roof and overlying rock to collapse into the void behind.

2.1. Correlation analysis between surface displacements and tilt caused by coal mining

The Stochastic Medium Theory Model (SMTM) is the most commonly used method for predicting the ground movements induced by coal mining activities (Litwiniszyn, 1974). It assumes that the rock mass can be moved from one location to another and its shape can vary under unit element mining, however its total volume remains the same, i.e., the sum of the normal strains in the x, y, and z directions (i.e. ε_x, ε_y, and ε_z, respectively) is equal to zero:

$$\varepsilon_x + \varepsilon_y + \varepsilon_z = 0 \tag{1}$$

The relationship between the tilt and horizontal displacement can be deduced based on Eq. (1):

$$U_e(x,y) = (b \cdot H/\tan\beta) \cdot I_e(x,y) \tag{2}$$

where $I_e(x,y)$ and $U_e(x,y)$ represent the tilt and the horizontal ground movement caused by exploiting the unit element considered, respectively. b, H and $tan\beta$ represent the coefficient of the horizontal movement, the mining depth of the extracted unit element, and the tangent of the major influential angle, respectively. However, it has been proved in many engineering applications that the proportional relationship indicated in Eq. (2) is only valid in a limited number of cases due to the fact that the main assumption of SMTM is inconsistent with the actual movement of rock mass. SMTM assumes that the total volume of overburden rock mass remains unchanged under coal mining, but the actual rock mass is anisotropic and discontinuous (with cracks), and its volume varies due to the bulk expansion and rheology of the rock mass during mining, i.e. the rock mass should be considered as a clastic medium. Therefore, the sum of the normal strains in the x, y, and z directions is not equal to zero: in the x-z plane, this relationship can be expressed as follows:

$$\varepsilon_x + \varepsilon_z = e(x,z) \neq 0 \tag{3}$$

where $e(x,z)$ is the function of the volume change of the rock mass related to the internal point (x, z) of the rock mass. ε_x and ε_z can be expressed as (Litwiniszyn, 1974):

$$\begin{cases} \varepsilon_x = \dfrac{\partial U_e(x,z)}{\partial x} \\ \varepsilon_z = \dfrac{\partial W_e(x,z)}{\partial z} \end{cases} \tag{4}$$

where $W_e(x, z)$ is the vertical ground subsidence caused by exploiting one unit element. Substituting Eq. (4) into Eq. (3), we have

$$\frac{\partial U_e(x,z)}{\partial x} + \frac{\partial W_e(x,z)}{\partial z} = e(x,z) \tag{5}$$

The ground horizontal movement U_e(x, z) caused by exploiting one unit element can be determined by integrating Eq. (5)

$$U_e(x,z) = \int_{-\infty}^{x} e(x,z)dx + \int_{-\infty}^{x} \frac{\partial W_e(x,z)}{\partial z}dx \tag{6}$$

Considering Eqs. (2), (6) can be expressed as

$$U_e(x,z) = B \cdot I_e(x,z) + F(x,z) \tag{7}$$

where B and $F(x, z)$ can be written as

$$\begin{cases} B = b \cdot \dfrac{H}{\tan \beta} \\ F(x,z) = \displaystyle\int_{-\infty}^{x} e(x,z)dx \end{cases} \tag{8}$$

and $F(x, z)$ is a function related to the rock deformation. To make the calculation easier, based on the measured results of surface-based observing station, $F(x, z)$ can be assumed as a linear function (Lian et al., 1994)

$$F(x,z) = \cot \theta \cdot W_e(x,z) \tag{9}$$

where θ is the propagation angle of the coal mine, i.e. the angle between the horizontal and the line passing through the maximum subsidence point and the center of extraction (see Fig. 1(b)). Therefore, the horizontal ground movement caused by exploiting unit element can be expressed as

$$U_e(x,z) = B \cdot I_e(x,z) + \cot \theta \cdot W_e(x,z) \tag{10}$$

Eq. (10) indicates that the surface displacement in the x direction caused by coal mining is not proportional to the tilt, but as the result of the superposition of the tilt and the vertical movement. The similar expression can also be deduced using the proposed theory in the y–z plane.

2.2. Modelling three-dimensional surface displacements of coal mining in time

As shown in Fig. 1(c), we take xOy as the local coordinate system on the Earth's surface and sO_1d as the coal mining coordinate system. Assuming that the unit element B (s, d) is exploited at time t, $W_e(x, y)$ is the corresponding vertical displacement of the surface point $A(x, y)$ caused by the unit element $B(s, d)$ and the vertical displacement $W(x, y, t)$ of point $A(x, y)$ at time t can be written as

$$W(x,y,t) = W_e(x,y) \cdot \psi(t) \tag{11}$$

where ψ(t) is a time influence function. According to Knothe's theory (Knothe, 1952), $W_e(x, y)$ and ψ (t) can be expressed as

$$\begin{cases} W_e(x,y) = 1/r^2 \cdot \exp\left(-\pi \cdot ((x-s)^2 + (y-d)^2)\big/r^2\right) \\ \psi(t) = 1 - e^{-ct} \end{cases} \tag{12}$$

where r is the major influence radius of the mining unit element $B(s, d)$, $r = H/\tan\beta$ as shown in Fig. 1(a). c is the coefficient of subsidence velocity and can be determined as

$$c = 2 \cdot v \cdot \tan \beta / H \tag{13}$$

where v is the mining velocity, i.e. the excavation distance of working panel per day, and is often considered as a constant for a given mine. Based on Eqs. (11), (12) and (13), the vertical displacement $W(x, y, t)$ of point $A(x, y)$ caused by the unit element B(s, d) at time t can be estimated precisely. Then the total vertical displacement of ground point $A(x, y)$ caused by the whole underground working zone at time t can be determined with the integral method, i.e. to divide the working panel into several unit elements, calculate the ground movement caused by each unit element according to Eq. (11) and then sum up all the ground movements of each unit element to obtain the total ground movement of the entire mined working panel. Thus the vertical displacement $W_a(x, y, t)$ of point $A(x, y)$ caused by the whole working panel can be expressed as

$$W_a(x,y,t) = \sum_{i=1}^{p} W(x,y,t) = \sum_{i=1}^{p} W_e(x,y) \cdot (1 - e^{-2 \cdot v \cdot t \cdot \tan \beta / H}) \tag{14}$$

where p is the number of unit elements and can be determined using Eq. (15) (Wu, 1995)

Fig. 1. (a) The geometric explanation of parameters r and β. $W(x)$ is the subsidence curve under semi-infinite mining condition, i.e. when time $t \to \infty$ and in $x > 0$, all the coal seam is exploited and in $x < 0$, the unmined coal seam remains. Surface deformation is mainly concentrated in the range of $2r$ above the mining boundary, this is the origin of parameter r; β is the angle between the horizontal and the line connecting the boundary point of the major influence range (i.e. $-r$ or r) and the mining boundary point. (b) Plane-coordinate system for coal mining. (c) Local coordinate systems for coal mining. Note that (i) parameters r, β, and H represent the major influence radius, major influence angle and mining depth. (ii) W_e represents the vertical displacement caused by exploiting one unit element, parameters θ and α represent the propagation angle of the coal mine and coal seam inclination, respectively. (iii) $B(s, d)$ represents one unit element, $A(x, y)$ represents one surface point influenced by exploiting unit element $B(s, d)$, $D1$ and $D2$ are the extraction length and width of the working panel, respectively.

$$p = \frac{D_1 \cdot D_2}{0.1 \cdot H \times 0.1 \cdot H} \tag{15}$$

where D_1 and D_2 represent the extraction length and width of working panel, respectively. As the tilt is the first spatial derivative of the vertical displacement (Litwiniszyn, 1974), the corresponding tilts ($I_{EW}(x, y, t)$ and $I_{NS}(x, y, t)$) of point $A(x, y)$ in the easting and northing directions at time t can be expressed as

$$\begin{cases} I_{NS}(x,y,t) = [W_a(x, y + 1, t) - W_a(x,y,t)]/\Delta y \\ I_{EW}(x,y,t) = [W_a(x + 1, y, t) - W_a(x,y,t)]/\Delta x \end{cases} \tag{16}$$

where Δx and Δy are the distance intervals of adjacent points in the easting and northing directions, respectively. The corresponding horizontal movements ($U_{EW}(x, y, t)$ and $U_{NS}(x, y, t)$) of point $A(x, y)$ in the easting and northing directions at time t can be determined using Eq. (10).

$$\begin{cases} U_{NS}(x,y,t) = (b \cdot H/\tan\beta) \cdot I_{NS}(x,y,t) + \cot\theta \cdot W_a(x,y,t) \\ U_{EW}(x,y,t) = (b \cdot H/\tan\beta) \cdot I_{EW}(x,y,t) + \cot\theta \cdot W_a(x,y,t) \end{cases} \tag{17}$$

In Eqs. (14), (15), (16) and (17), parameters v, H, D_1, D_2, Δx, Δy are all constants over a continuous coal mining area. Parameters $\tan\beta$, θ and b are the variables over time. Therefore, 3D surface displacements can be derived when parameters $\tan\beta$, θ and b are known. This offers a great opportunity to retrieve 3D deformation from SAR images with a single imaging geometry.

2.3. Estimating model parameters using time-varying OT results

It is clear from Section 2.2 that 3D time-varying movements can be retrieved when parameters $\tan\beta$, θ and b are known. Here a method is proposed to determine the dynamic parameters $\tan\beta$, θ and b using time-varying OT results. To obtain time-varying OT results, multiple SAR images (assuming m images in total) are first paired to form n pairs, and the range displacements $\boldsymbol{R} = [r_1, r_2, …, r_n]^T$ are computed for all the SAR pairs using OT. The following equation is constructed to obtain the time-varying displacements

$$BX = R \tag{18}$$

where $\boldsymbol{X} = [x_1, x_2, …, x_{m-1}]^T$ are the time-varying surface displacements in the LOS direction that needs to be solved, and B is a coefficient matrix with a dimension of $n \times (m-1)$. As $n \geq m-1$ and the rank of B is $m-1$, Eq. (18) can be solved using the least squares (LS) method

$$X = (B^T B)^{-1} B^T R \tag{19}$$

An iteration method is used to estimate parameters $\tan\beta$, θ and b as follows:

Step 1. To determine the initial vertical displacements with an assumption of no horizontal movement at time t. The vertical displacement of an arbitrary pixel (i, j) at time t can be determined as:

$$W(i,j,t) = LOS(i,j,t)/\cos(\phi(i,j)) \tag{20}$$

where ϕ is the radar incidence angle, $W(i, j, t)$ is the vertical displacement of pixel (i, j) at time t and $LOS(i, j, t)$ is the OT derived range displacement of pixel (i, j) at time t.

Step 2. To estimate parameters $\tan\beta$, θ and b using the Genetic Algorithm Optimization Toolbox (GAOT) developed at North Carolina State University. The basic idea of Genetic Algorithm (GA) is to select the "chromosomes" that are more suitable for the environment to generate a new offspring. After many times of evolution, they finally converge and acquire a "chromosome" that best fits the environment and this population is the optimal solution to the problem (Holland, 1975). The value range of each parameter is firstly assigned according to the specific geology and mining conditions. Then the initial parameter population is generated by ordering the parameters into chromosome strings in which each gene represents one parameter, i.e. $\tan\beta$,

θ and b. GA is then used to generate a new generation of chromosome groups that are more adaptable to the environment. The chromosome groups are evolved from generation to generation and finally the ones that best adapt to the environment, i.e. the prediction results with the smallest variances (here compared with GPS measurements) are chosen as the final parameters.

Step 3. To estimate the initial 3D surface displacements. Based on the parameters obtained in Step 2, 3D displacements can be estimated using Eqs. (14), (16) and (17).

Step 4. To simulate the range displacements based on the 3D model in Step 3. The simulated range displacement LOS′(i, j, t) can be obtained using the following equation

$$\begin{aligned} LOS'(i,j,t) = W(i,j,t) \cdot \cos(\phi(i,j)) - \sin(\phi(i,j)) \\ \cdot [U_{NS}(i,j,t) \cdot \cos(\delta - 3\pi/2) + \\ U_{EW}(i,j,t) \cdot \sin(\delta - 3\pi/2)] \end{aligned} \tag{21}$$

where δ is the radar heading angle, $U_{NS}(i, j, t)$ and $U_{EW}(i, j, t)$ are the horizontal displacements of pixel (i, j) in the northing and easting directions respectively, at time t. Then the absolute residual ΔLOS $(i,j,t) = |LOS'(i,j,t) - LOS(i,j,t)|$ is generated.

Step 5. To compare the absolute residual with a given threshold ε, here set as 10 mm. (i) If $\Delta LOS(i, j, t) \leq \varepsilon$, output the parameters $\tan\beta$, θ and b and the time-varying 3D displacements from Eqs. (14), (16) and (17). (ii) If $\Delta LOS(i, j, t) > \varepsilon$, then correct the original LOS displacement, i.e. $LOS''(i, j, t) = LOS(i, j, t) + \Delta LOS(i, j, t)$, where $LOS''(i, j, t)$ is the corrected LOS displacement of pixel (i, j) at time t and will be used to calculate the vertical displacement in Step 1.

Step 6. To repeat Steps 1 to 5 until the absolute residual $\Delta LOS(i, j, t)$ is within the given threshold ε, and output the parameters $\tan\beta$, θ and b and the time-varying 3D displacements from Eqs. (14), (16) and (17).

Since the 3D time-varying large surface displacements are derived from OT measurements and clastic medium theory (CMT), hereafter this method is referred as OT-CMT. The flow chart of OT-CMT is shown in Fig. 2.

3. Case study

3.1. Study area and data used in this study

The study area is located in the Daliuta coal mining area, Shaanxi Province, China. With thick loose layers, shallow coal seams, thin bedrock, a small mining depth to mining thickness ratio, and fast advancement of the working panel, this region is characterized by large ground movements. Ground movement due to coal mining has unique features, including the fast propagation of coal mining influences, discontinuous surface displacements, and a large probability of catastrophes such as stepped collapses, hillside slip and landslides. A single reference real-time kinematic (RTK) GPS was used to collect the coordinates of 71 ground stations along the strike (direction of the line formed by the intersection of coal seam with a horizontal plane) and dip (direction of the line formed by the intersection of coal seam with a vertical plane perpendicular to the strike of the feature) directions on the coal mine working panel (Fig. 3). The green circles in Fig. 3 represent the 45 GPS stations along the strike direction with a station spacing of 20 m, and the 26 GPS stations along the dip direction with a station spacing of 25 m, 71 GPS monitoring points in total. GPS results show the maximum subsidence of about 4.4 m in the study area during the period from November 2012 to April 2013. Such large surface displacements make it a big challenge to use InSAR in this case.

The working panel in the study area has a length of approximately 4547 m and a width of approximately 300 m, with an average mining depth of about 235 m and a coal seam inclination of approximately 1° to 3°. Most of the ground surface is covered by Quaternary unconsolidated sediments with an average thickness of 30 m. The overlying bedrock
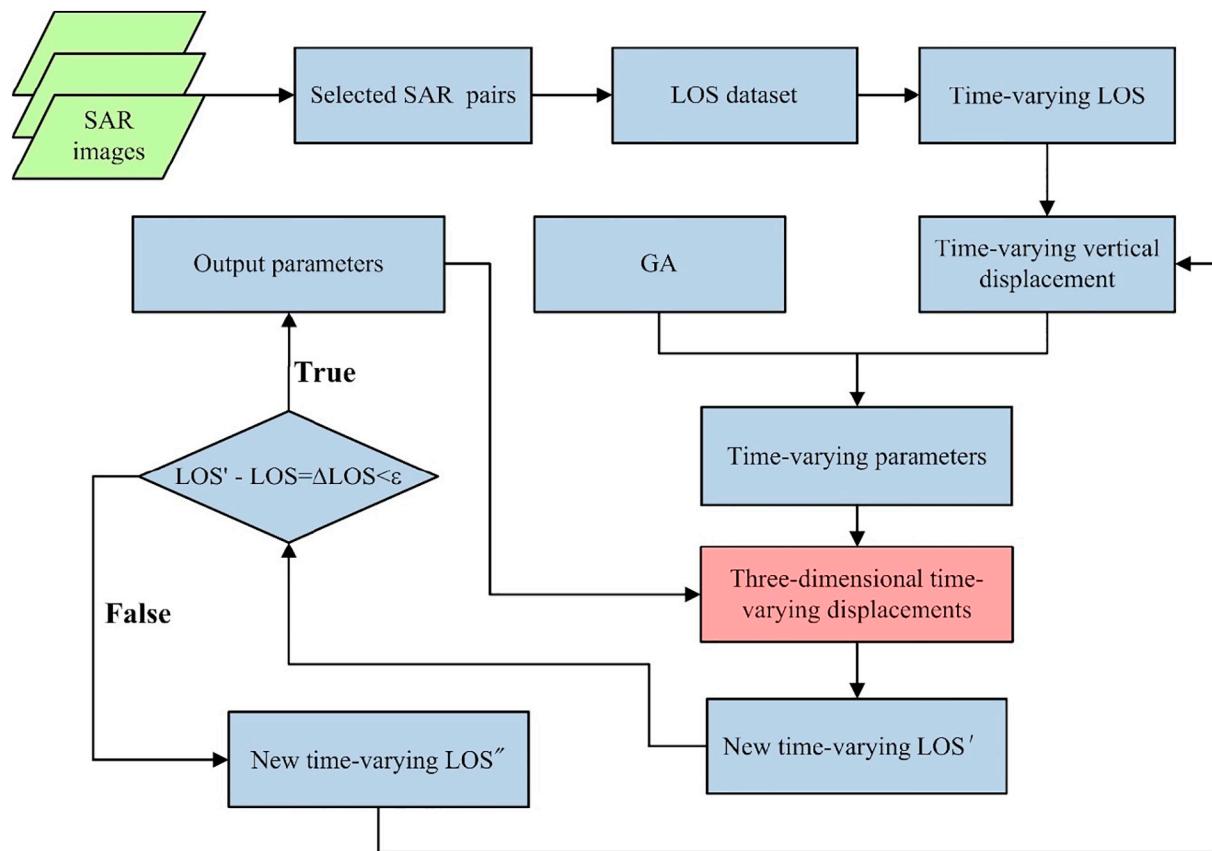
Fig. 2. The flow chart of the OT-CMT method.

primarily consists of siltstones and fine sandstones, with an average depth of about 200 m. Coal mining started on November 1, 2012 and terminated on March 25, 2013 along the southeast-northwest direction.

Chen and Deng (2014) used conventional InSAR to obtain LOS surface displacements in the same site, and they applied interpolation to the central deforming area where large surface displacements were
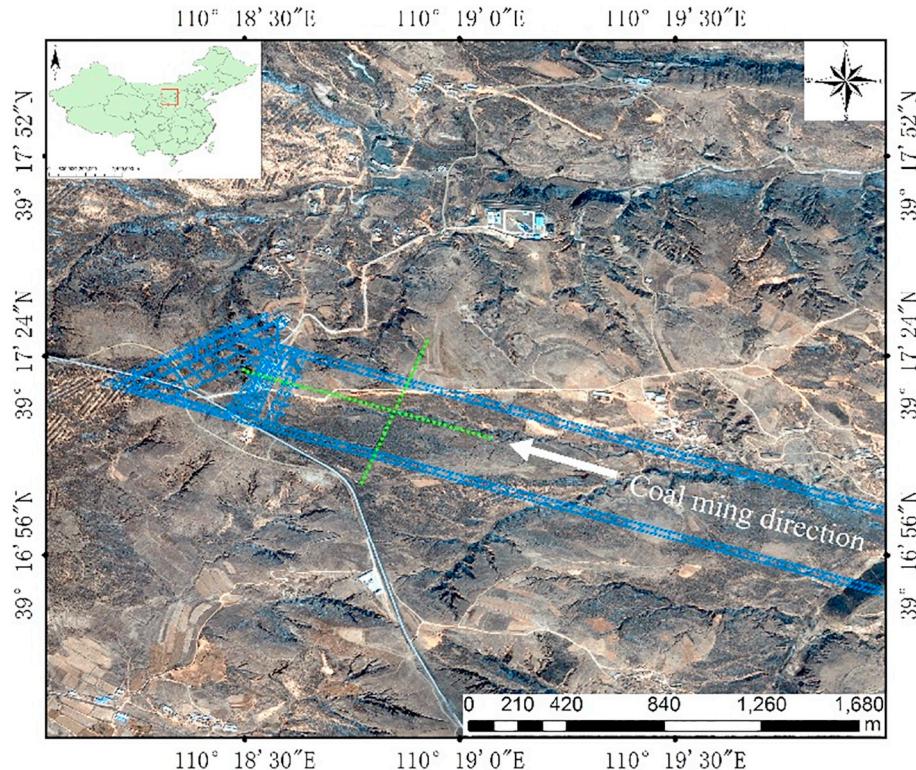
Fig. 3. The study area with the coal mine working panels. Note that green circles represent the GPS stations, blue polygons represent the working panels, and the white arrow represents the mining direction. (For interpretation of the references to colour in this figure legend, the reader is referred to the web version of this article.)

Table 1
TerraSAR-X images used in this study.

Acquisition date	Perpendicular baseline (m)	Temporal baseline (days)	Doppler central frequency (HZ)
2012/11/21	−34.10	77	2885
2012/12/02	−171.73	66	2892
2012/12/13	−149.38	55	2914
2012/12/24	−51.92	44	2897
2013/01/04	8.70	33	2921
2013/01/15	82.91	22	2820
2013/01/26	20.28	11	3024
2013/02/06	0	0	3310
2013/02/17	−117.89	11	3359
2013/02/28	−26.06	22	3265
2013/03/11	51.97	33	3334
2013/03/22	116.73	44	3306
2013/04/02	−38.41	55	3341

evident. Fan et al. (2015) collected 3D large ground movements at Daliuta mining area using OT and PIM. However, in their analysis they assumed that there was no horizontal movement, which did not hold true; moreover, it only managed to estimate the total surface displacements but failed to recover the evolution of the ground motion during the whole coal mining period. Yang et al. (2018) proposed to use OT with PIM to derive the time-series of 3D surface displacements in the Daliuta coal mining area. However, as mentioned in Section 1, their assumed model might not be consistent with the actual ground motion. Therefore, we attempt to use SAR data to further investigate the evolution of the surface displacements of Daliuta coal mining area in this study. As shown in Table 1, 13 scenes of high resolution Spotlight TerraSAR-X images with an azimuth pixel spacing of 0.85 m and a range pixel spacing of 0.91 m were used to extract surface displacements. These images were acquired during the period from November 21, 2012 to April 2, 2013, which spanned the same period as the actual mining activity.

3.2. 3D surface displacements in time

3.2.1. OT-CMT results

OT-CMT was employed to obtain the dynamic 3D surface
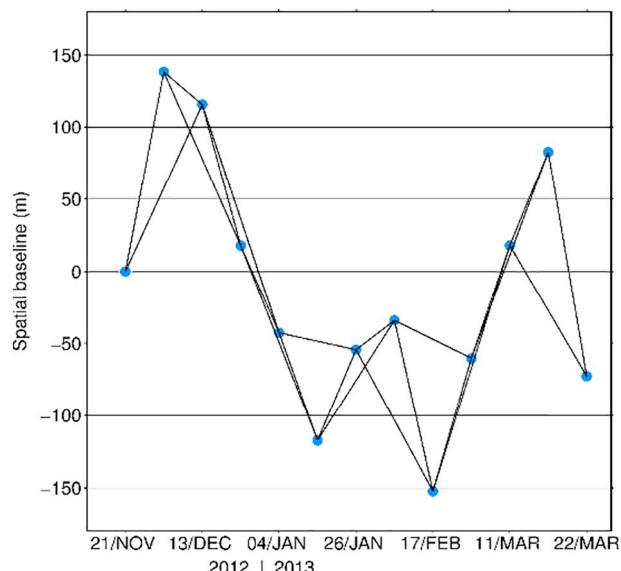
Fig. 4. Spatial and temporal baselines of the selected TerraSAR-X pairs.

displacements in the study area. First, a common master image (for this study 2013/02/06) was selected according to the Doppler central frequencies and the spatial and temporal baselines (Table 1), and the remaining images were registered to the master image. To remove the topographic phase contributions, the 1-arcsecond (~30 m) spacing Shuttle Radar Topography Mission (SRTM) Digital Elevation Model (DEM) was used (Farr et al., 2007; NASA, 2015). To ensure good coherence, the temporal baseline threshold was set to 22 days, and 23 pairs (Fig. 4) were processed to generate range displacement maps with the OT technique. To maximize the correlation values while taking into account the computation efficiency, the search window in the OT computation process was set to 64 × 64 pixels and the oversampling factor was set to 2. The time-varying range displacements were generated via Eq. (19). Note that the azimuth offsets were also calculated but they were seriously affected by ionospheric disturbance; therefore the azimuth offsets were not used in further analysis in this study. Finally, the 3D displacement model was constructed using the OT-CMT approach introduced in Section 2.2. Here the radar incidence angle ϕ is 42.43° and the heading angle α is 189.53° for TerraSAR-X. Parameters b, $\tan\beta$ and θ were obtained via the GA method with 50 populations and 200 generations. To eliminate the influence of the random errors caused by the GA method, all the parameters were optimized by GA independently 200 times at each time interval, and the corresponding average (AVG) values were accepted as the final values. The statistical distributions of parameters $\tan\beta$, b and θ and corresponding AVG and standard error (STD) are illustrated in Fig. 5(a)–(c), which show approximately normal distributions and demonstrate the rationale to take the mean values. Fig. 5(d)–(f) show the temporal variations of parameters $\tan\beta$, b and θ, respectively, illustrating that all the parameters are in a dynamic state over time.

Fig. 6(a) illustrates the maximum vertical surface displacement of approximately 4.5 m during the period from November 21, 2012 to April 2, 2013. The ground movements accumulated gradually from the southeast to northwest which is consistent with the exploiting direction of the mine workings, with a transformation from a bowl shape (in plain view) into an elliptical area of displacement. Fig. 6(b) and (c) show that the maximum horizontal movements of approximately 1.4 m and 1.2 m in the northing and easting directions during the period from November 21, 2012 to April 2, 2013, respectively. In Fig. 6(c), three distinct areas moved towards the East and one area moved towards the West in the working panel. A comparison between Fig. 6(b) and (c) show that the maximum horizontal movement in the northing direction is greater than that in the easting direction and the horizontal movements in the northing direction is nearly symmetric. In addition, Fig. 6(b) and (c) show that the horizontal displacements towards the subsidence centre have negligible displacement and the maximum horizontal movement occurred at the edges of the mining area and diminished towards the outer space.

To further analyse the evolution of ground movement, the time-varying vertical and horizontal surface displacement profiles along AA′ and BB′ are shown in Fig. 5. Fig. 5(g) and (h) suggest that the horizontal movement curves for Profile AA′ fluctuate considerably in different periods with a maximum negative movement of −665.0 mm and a maximum positive movement of +615.0 mm. Fig. 5(i) shows that with the exploiting of the working panel, ground subsidence along profile AA′ increases dramatically, which results in the rapid formation of a collapsed basin. From November 21, 2012 to January 4, 2013, the ground subsided dramatically and reached 2.569 m, accounting for 58.4% of the final maximum ground subsidence of 4.43 m.

Compared to the fluctuant pattern of horizontal movement curves for Profile AA′, the horizontal surface displacement curves for Profile BB′ (Fig. 5(j) and (k)) formed two symmetric regions: negative movement with a maximum of −676.0 mm and positive movement with a maximum of +704.0 mm. Compared to the characteristics of ground
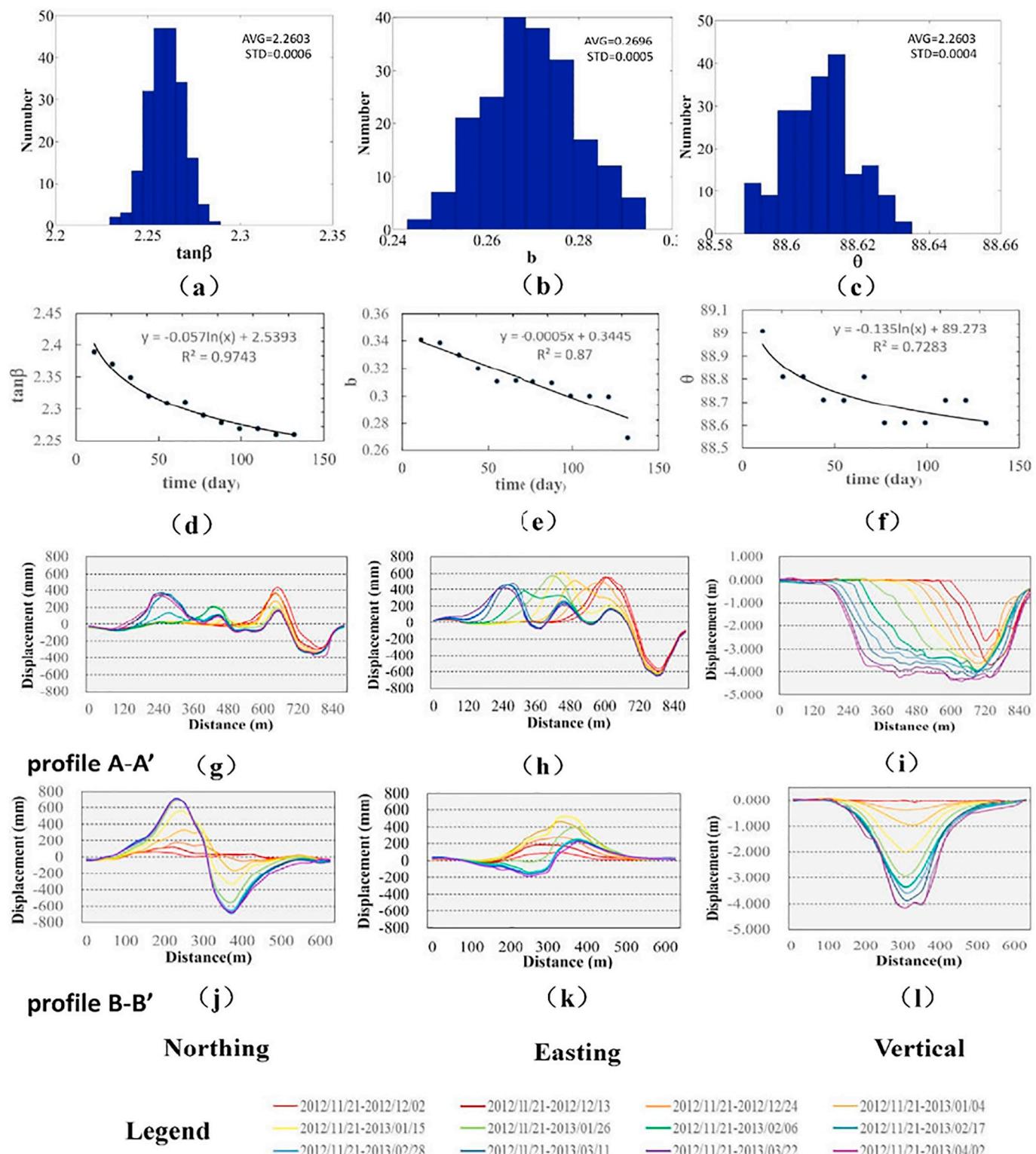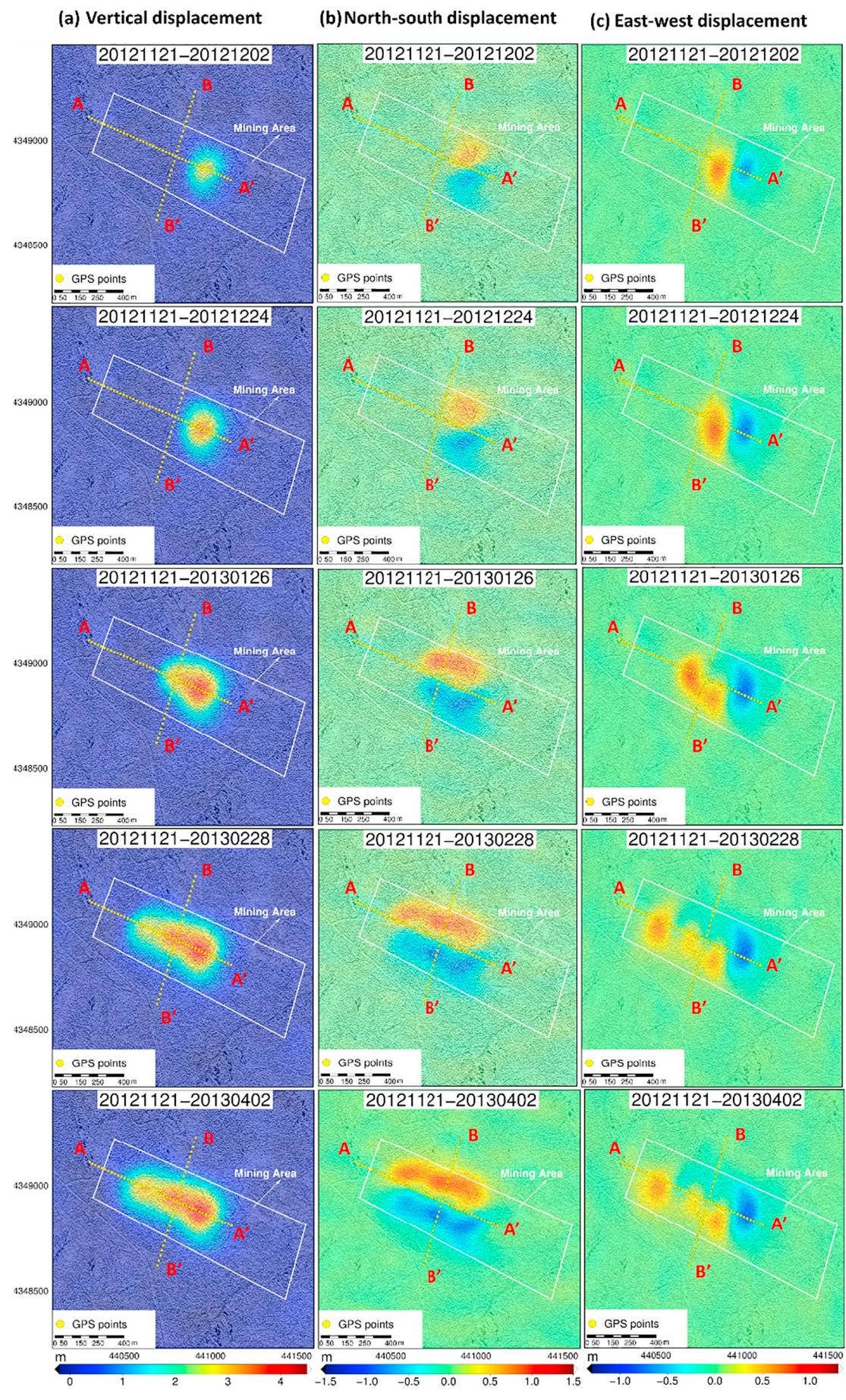
Fig. 5. (a)–(c) are the statistical distributions of parameters tanβ, b and θ between November 21, 2012 and April 2, 2013, respectively. (d)–(f) are the temporal variations of parameters tanβ, b and θ, respectively. Note that parameters tanβ and b are dimensionless and parameter θ is in degrees. (g)–(i) are the time-varying northing, easting and vertical surface displacements along Profile AA′, respectively. (j)–(l) are the time-varying northing, easting and vertical surface displacements along Profile BB′, respectively.

subsidence along profile AA′, ground subsidence curves along Profile BB′ (Fig. 5(l)) showed a different pattern, which increased slightly during the period from November 21, 2012 to January 4, 2013 and increased dramatically by 2.056 m, accounting for 49.5% of the final maximum ground subsidence (the maximum subsidence was 4.157 m)

during the period from January 4, 2013 to January 26.

3.2.2. Validation

To evaluate the OT-CMT results, 852 GPS measurements over the 71 monitoring stations (Fig. 3) collected in 12 RTK GPS campaigns during

(a) Vertical displacement (b) North-south displacement (c) East-west displacement

(caption on next page)

Fig. 6. (a)–(c) are the accumulative surface displacements in the vertical, northing and easting directions, respectively. Note that (i) positive vertical displacements represent ground subsidence and negative displacements represent ground uplifts; (ii) positive horizontal displacements represent the Earth's surface moved towards the northing and easting direction, respectively; and (iii) only 5 out of 12 cumulative deformation maps are shown in the vertical, northing and easting directions, respectively.
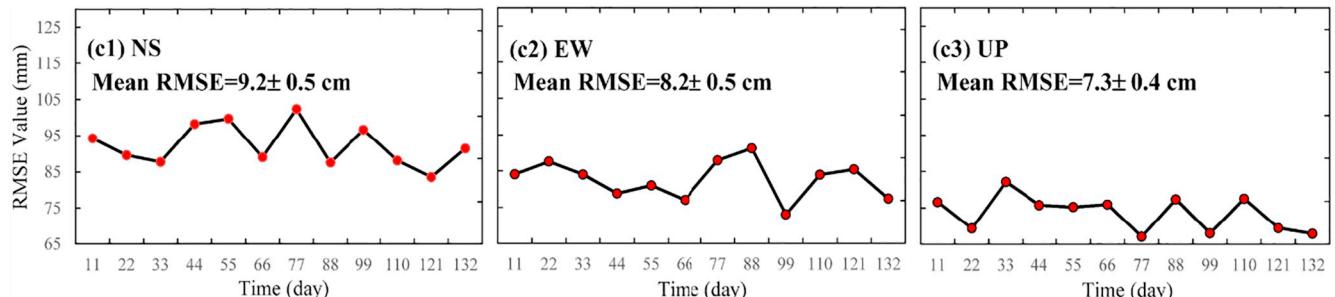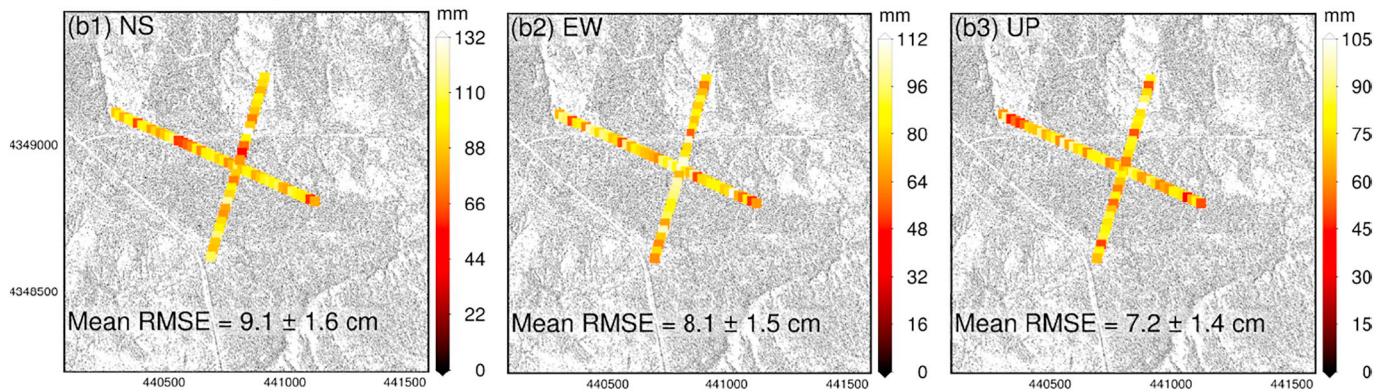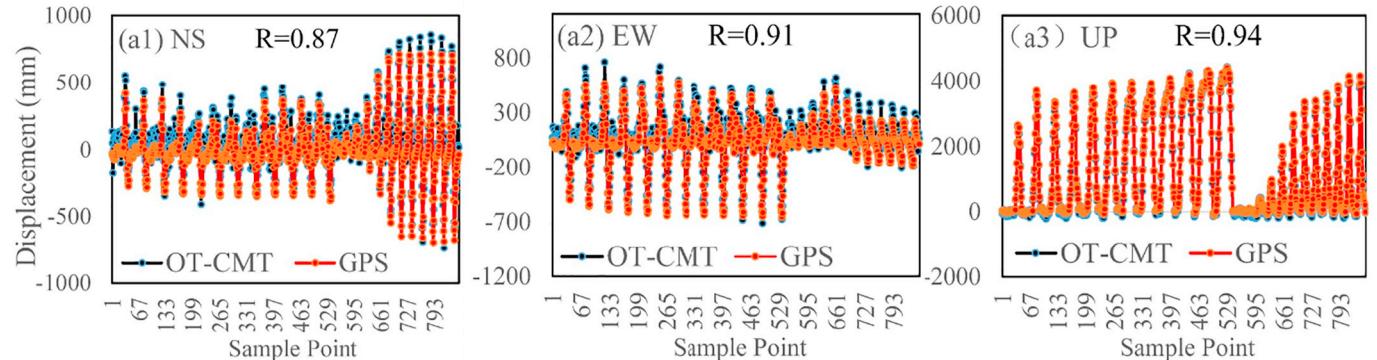
Fig. 7. (a1)-(a3) are the spatial-temporal comparisons between OT-CMT and GPS surface displacements. (b1)-(b3) are the spatial comparisons between OT-CMT and GPS surface displacements. (c1)-(c3) are the temporal comparisons between OT-CMT and GPS surface displacements. Note that (i) the time span is from 21 November 2012 to 2 April 2013, in which 12 RTK GPS campaigned were carried out with a time interval of 11 days (corresponding to TerraSAR-X acquisitions, Table 1) and therefore the total number of GPS measurements is $71 \times 12 = 852$; and (ii) all the comparisons were performed in the northing, easting and vertical directions, respectively.

the period from 21 November 2012 to 2 April 2013 were used as "the truth" with precision of about 1 cm in the easting and northing directions and 2 cm in the vertical direction. The corresponding spatial-temporal root-mean-square errors (RMSEs), spatial RMSEs and temporal RMSEs of the OT-CMT results were calculated (Fig. 7). The RMSEs in the vertical direction are the smallest, i.e.7.4, 7.2 and 7.3 cm in the spatial-temporal, spatial and temporal comparisons, respectively; the RMSEs in the easting direction are the second smallest, i.e. 8.3, 8.1 and 8.2 cm; and the RMSEs in the northing direction are the largest, i.e. 9.3, 9.1 and 9.2 cm. The relative RMSEs against the maximum GPS measurements are 1.7%, 13.2% and 13.5% in the vertical (about 4.43 m), northing (about 0.704 m) and easting (about 0.615 m) directions, respectively. Such accuracy can satisfy the practical and legal requirements of the coal mining industry (State Bureau of Coal Industry, 2000). Yang et al. (2018) proposed to combine OT with PIM to derive

3D surface displacement time-series in the Daliuta coal mining area and they reported that RMSEs of 11 cm and 22 cm in the horizontal and vertical directions, respectively. Note that, for the convenience of comparison with this previous study, here the horizontal movements are obtained by synthesizing the movements in the northing and easting directions and a 7.7 cm RMSE of the retrieved horizontal displacements against GPS was obtained. Compared with Yang et al. (2018), the performance of our OT-CMT approach has improved accuracy about 30% and 58% in horizontal and vertical directions, respectively.

3.3. Prediction of mining-induced ground movements

The stress changes in the rock stratum can lead to ground movements, which is a complex process and can evolve in space and time. Prediction models of surface displacements are desirable to predict
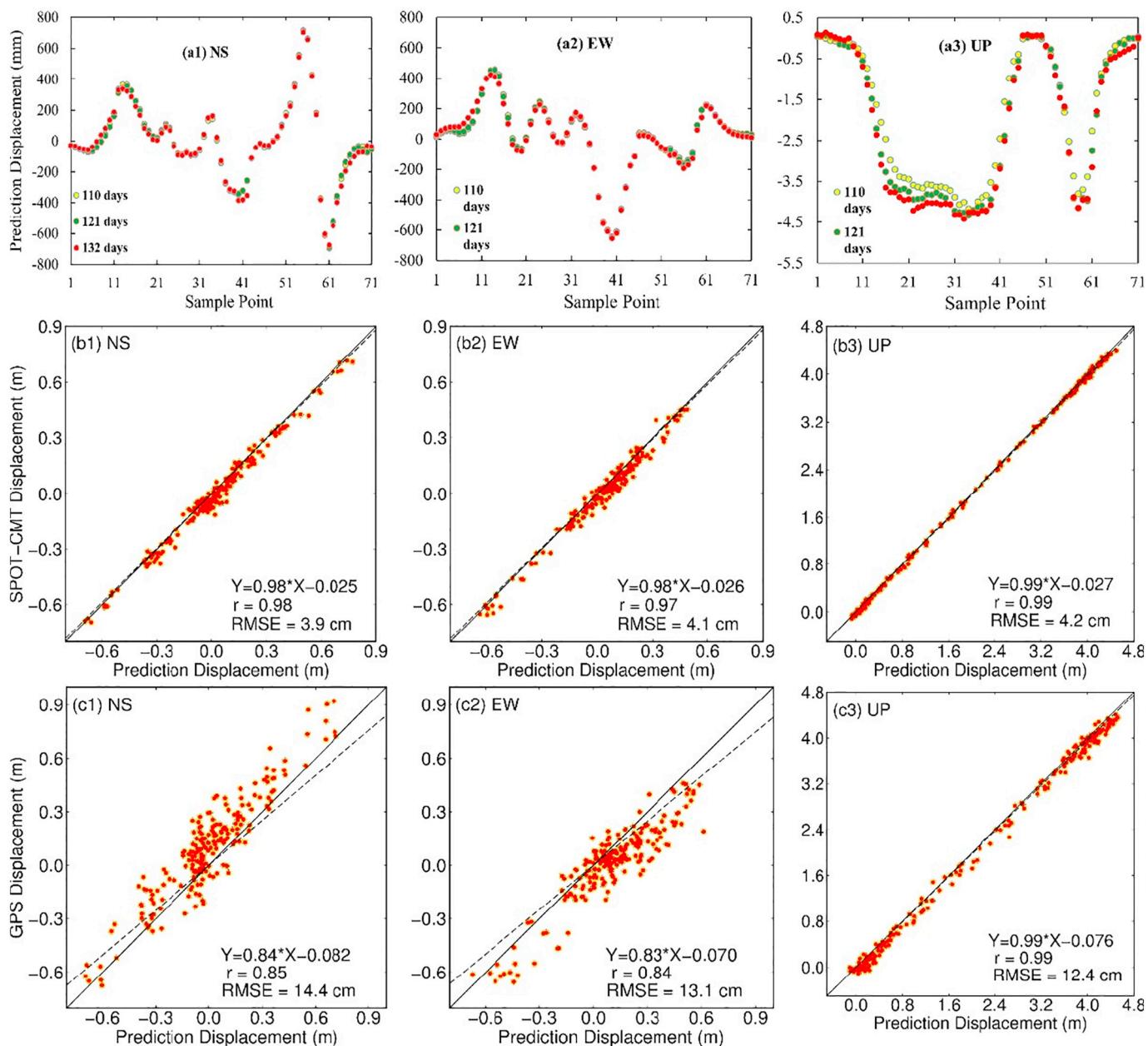
Fig. 8. (a1)-(a3) are the time series of the predicted displacements by SVR. The legends '110 days', '121 days' and '132 days' refer to the start date of 21 November 2012. (b1)-(b3) are the spatial-temporal comparisons between the predicted and OT-CMT displacements. (c1)-(c3) are the spatial-temporal comparisons between predicted and GPS displacements. Note that all the comparisons results are performed in the northing, easting and vertical directions, respectively. The line of perfect fit (solid line) and a least squares regression line (dashed line) are plotted. The number of the test samples is 213 during the period from 11 March 2013 to 2 April 2013.

future mining-induced ground movements, and hence reduce the probability and loss of disaster occurrence.

In this study the Support Vector Regression (SVR) algorithm (Burges, 1998; Smola and Schölkopf, 2004) was employed to describe the nonlinear relationship between the measured and future surface displacements. The OT-CMT results can be considered as many groups of time-related discrete data, and can be used to constitute a nonlinear time series $\{x_i\} = \{x_1, x_2, \dots x_n\}$, where n is the number of the measured surface displacements (Chen and Deng, 2014).

To predict the surface displacement x_{i+p} at time point $i + p$, one must find a function $x_{i+p} = f(x_i, x_{i+1}, \dots, x_{i+p-1})$ to describe the relationship between x_{i+p} and the previous p measured displacements, where $i = 1,2, \dots, n-p$, and p represents the size of the input vector. The nonlinear time series can then be transformed to the following two matrices:

$$X = \begin{bmatrix} x_1 & x_2 & \cdots & x_p \\ x_2 & x_3 & \cdots & x_{p+1} \\ \cdots & \cdots & \cdots & \cdots \\ x_{n-p} & x_{n-p+1} & \cdots & x_{n-1} \end{bmatrix}, Y = \begin{bmatrix} x_{p+1} \\ x_{p+2} \\ \cdots \\ x_n \end{bmatrix} \tag{22}$$

We used matrices X and Y as the training and learning samples to establish the SVR function $Y = f(x)$, which can be expressed as follows:

$$f(x_t) = \sum_{i=1}^{n-p} (a_i - a_i^*) K(x_i \cdot x_t) + b, \quad t = p + 1, \dots n. \tag{23}$$

where $K(\cdot)$ represents the kernel function, a_i and a_i^* are the Lagrangian multipliers, and b is a constant. For greater details of the SVR approach, please refer to Chen and Deng (2014).

Since the surface deformation caused by underground coal mining is a complex space-time evolution process, it is expected that the function

itself should have the ability to update the samples to adjust the predicted value in real time. But the SVR algorithm itself is a static prediction, and the predicted value cannot be dynamically adjusted according to the changing conditions. In order to make full use of the latest displacement information to improve the prediction performance, we employed a rolling prediction method (Chen and Deng, 2014) to update the training sample data and thus constitute a dynamic prediction model. Here the monitoring data of ground observations obtained by OT-CMT along Profiles AA′ and BB′ were selected for validation purposes, i.e. 45 points along the strike direction and 26 points along the dip direction (see the ground observations in Fig. 3). We used the measured data from 21 November 2012 to 28 February 2013 (nine groups) as the training and learning samples for SVR and took the measured data from 11 March to 2 April 2013 as the test samples to assess the performance of the prediction model.

As demonstrated in Chen and Deng (2014), the optimal parameters can be selected according to the final prediction residuals. In this study, the size of the input vector was set to 4 and the step size of the prediction was set to 1 (i.e. 11 days) to establish the prediction function f (·). Based on the prediction function with optimal parameters, the rolling prediction method was used to predict the surface displacements step-by-step and their predicted results are shown in Fig. 8(a1)-(a3), respectively. Fig. 8(a1)-(a3) show that the shapes of all the predicted time series are similar to Fig. 5 and also the maximum displacement values are consistent with the OT-CMT results in the northing, easting and vertical directions, respectively.

Fig. 8(b1)-(b3) show that there are high correlations between the predicted and the OT-CMT displacements with RMSEs ranging from 3.9 to 4.2 cm in the three directions, demonstrating the robustness of the rolling prediction method. Fig. 8(c1)-(c3) illustrate that the correlations are smaller and the RMSEs are greater than those in Fig. 8(b1)-(b3); the corresponding RMSEs are 14.4, 13.1 and 12.4 cm in the northing, easting and vertical directions, respectively. The reason for the lower correlations and larger RMSEs in Fig. 8(c1)-(c3) can be explained as the error propagation caused by the OT-CMT results. The predicted results can provide risk warnings and promote strategic decision-making for engineering management in the process of coal mining.

4. Conclusions

Coal mining often leads to large surface displacements with high spatial gradients, which is beyond the detection ability of traditional InSAR. Surface displacements caused by underground coal mining occur in both the horizontal and vertical directions, but traditional InSAR only provides observations in the radar line of sight. In this paper, a new approach has been demonstrated to extract 3D surface displacements, caused by underground coal mining, through the combination of SAR pixel offset tracking technique with coal mining subsidence theory. There are several obvious advantages of the OT-CMT approach: (i) surface displacements with large spatial gradients can be obtained; (ii) SAR images with a single imaging geometry only are required; and (iii) the evolution of 3D surface displacements can be determined.

In addition, the SVR algorithm is employed to develop an early prediction model. The framework demonstrated in this paper is not only able to derive the evolution of the 3D large surface displacements with multi-temporal SAR images with a single imaging geometry, but also to provide risk warnings and promote strategic decision-making for engineering management in the process of coal mining.

This study has considered one mining subsidence area in a specific type of geology and mining method. Mining subsidence with different topography, different mining depth and coal seam inclination may present different movement behaviours and require different forms of analysis. Thus, application of the proposed method to more mining subsidence cases (including different topography, different mining depth and coal seam inclination, etc.) with different SAR geometries

should be the focus of future studies. Coal mining subsidence is a complex temporal-spatial process and in this case study an exponential function model was employed which might not perform well for different types of surface deformation process. So future work should also focus on the improvement of the assumed time-related function of coal mining.

CRediT authorship contribution statement

Bingqian Chen: Conceptualization, Methodology, Writing - original draft. **Zhenhong Li:** Supervision, Conceptualization, Writing - review & editing. **Chen Yu:** Validation, Visualization. **David Fairbairn:** Writing - review & editing. **Jianrong Kang:** Resources, Project administration. **Jinshan Hu:** Investigation, Validation.**Liang Liang:**Investigation, Validation.

Declaration of competing interest

The authors declare that they have no known competing financial interests or personal relationships that could have appeared to influence the work reported in this paper.

References

Barbato, J., Hebblewhite, B., Mitra, R., Mills, K., 2016. Prediction of horizontal movement and strain at the surface due to longwall coal mining. Int. J. Rock Mech. Min. Sci. 84, 105–118. https://doi.org/10.1016/j.ijrmms.2016.02.006.
Burges, C.J.C., 1998. A tutorial on support vector machines for pattern recognition. Data Min. Knowl. Discov 2, 121–167. https://doi.org/10.1023/a:1009715923555.
Casu, F., Manconi, A., Pepe, A., Lanari, R., 2011. Deformation time-series generation in areas characterized by large displacement dynamics: the SAR amplitude pixel-offset SBAS technique. IEEE Trans. Geosci. Remote Sens. 49, 2752–2763. https://doi.org/10.1109/TGRS.2010.2104325.
Chen, B.Q., Deng, K.Z., 2014. Integration of D-InSAR technology and PSO-SVR algorithm for time series monitoring and dynamic prediction of coal mining subsidence. Surv. Rev. 46, 392–400. https://doi.org/10.1179/1752270614Y.0000000126.
Fan, H., Gao, X.X., Yang, J.K., Deng, K.Z., Yu, Y., 2015. Monitoring mining subsidence using a combination of phase-stacking and offset-tracking methods. Remote Sens. 7, 9166–9183. https://doi.org/10.3390/rs70709166.
Farr, T.G., Rosen, P.A., Caro, E., Crippen, R., Duren, R., Hensley, S., et al., 2007. The shuttle radar topography Mission. Rev. Geophys. 45, RG2004. https://doi.org/10.1029/2005RG000183.
Guo, G.L., Zhu, X.J., Zha, J.F., Wang, Q., 2014. Subsidence prediction method based on equivalent mining height theory for solid backfilling mining. Trans. Nonferrous Metals Soc. China 24, 3302–3308. https://doi.org/10.1016/S1003-6326(14)63470-1.
Guo, Q.B., Guo, G.L., Lv, X., Zhang, W.X., Lin, Y.K., Qin, S.Y., 2016. Strata movement and surface subsidence prediction model of dense solid backfilling mining. Environ. Earth Sci. 75, 1426. https://doi.org/10.1007/s12665-016-6237-6.

He, G.Q., 1985. The movement and deformation calculation of undermined anisotropic rock massif. In: Proceeding of 6th International Congress International Society for Mine SurveyingHarrogate.

He, G., Ma, W.M., 1985. Distribution laws and error control of rock and surface horizontal movement caused by underground mining. In: Proceeding of 6th International Congress International Society for Mine Surveying. Harrogate.

Holland, J.H., 1975. Adaptation in Natural and Artificial Systems. University of Michigan Press.

Howladar, M., Hasan, K., 2014. A study on the development of subsidence due to the extraction of 1203 slice with its associated factors around Barapukuria underground coal mining industrial area, Dinajpur, Bangladesh. Environ. Earth Sci. 72, 3699–3713. https://doi.org/10.1007/s12665-014-3419-y.

Huang, J.L., Deng, K.Z., Fan, H.D., Yan, S.Y., 2016. An improved pixel-tracking method for monitoring mining subsidence. Remote Sens. Lett. 7, 731–740. https://doi.org/10.1080/2150704x.2016.1183177.

Knothe, S., 1952. Time influence on a formation of a subsidence surface. Archiwum Gómictwa i Hutnictwa, Kraków 1, 1–3.

Li, L.J., 2006. Mine collapse and economic transformation in the cities with coal mine. Acad. J. Jinyang 5, 56–60. https://doi.org/10.16392/j.cnki.14-1057/c.2006.05.010.

Li, Z.H., Elliott, J.R., Feng, W.P., Jackson, J.A., Parsons, B.E., Walters, R.J., 2011. The 2010 MW 6.8 Yushu (Qinghai, China) earthquake: constraints provided by InSAR and body wave seismology. J. Geophys. Res. Solid Earth 116 (B10), B10302. https://doi.org/10.1029/2011JB008358.

Lian, C.J., Guo, W.J., Liu, L.M., 1994. Study on the law and prediction menthod of strike horizontal displacement by mining. Chin. J. Rock Mech. Eng. 13 (2), 141–148.

Litwiniszyn, J., 1974. Stochastic methods in mechanics of granular bodies. In: Litwiniszyn, J. (Ed.), Stochastic Methods in Mechanics of Granular Bodies: Course Held at the Department of General Mechanics. Springer Vienna, Vienna, pp. 5–9. https://doi.org/10.1007/978-3-7091-2836-7.

Massonnet, D., Feigl, K.L., 1998. Radar interferometry and its application to changes in the Earth's surface. Rev. Geophys. 36, 441–500. https://doi.org/10.1029/97RG03139.

Massonnet, D., Rossi, M., Carmona, C., Adragna, F., Peltzer, G., Feigl, K., Rabaute, T., 1993. The displacement field of the Landers earthquake mapped by radar interferometry. Nature 364, 138–142. https://doi.org/10.1038/364138a0.

Michel, R., Avouac, J.P., Taboury, J., 1999. Measuring ground displacements from SAR amplitude images: application to the Landers earthquake. Geophys. Res. Lett. 26, 875–878. https://doi.org/10.1029/1999gl900138.

NASA, 2015. NASA SRTM Version 3.0 Global 1 Arc Second Dataset. https://lpdaac.usgs.gov/documents/179/SRTM_User_Guide_V3.pdf.

Nie, L., Wang, H.F., Xu, Y., Li, Z.C., 2015. A new prediction model for mining subsidence deformation: the arc tangent function model. Nat. Hazards 75, 2185–2198. https://doi.org/10.1007/s11069-014-1421-z.

Reddish D J, Whittaker B N. Subsidence: occurrence, prediction and control[M]. Elsevier, 2012.

Sánchez-Gámez, P., Navarro, F., 2017. Glacier surface velocity retrieval using D-InSAR and offset tracking techniques applied to ascending and descending passes of Sentinel-1 data for Southern Ellesmere ice caps, Canadian Arctic. Remote Sens. 9, 442. https://doi.org/10.3390/rs9050442.

Salmi, E.F., Nazem, M., Karakus, M., 2017. The effect of rock mass gradual deterioration on the mechanism of post-mining subsidence over shallow abandoned coal mines. Int. J. Rock Mech. Min. Sci 91, 59–71.

Singleton, A., Li, Z.H., Hoey, T., Muller, J.P., 2014. Evaluating sub-pixel offset techniques as an alternative to D-InSAR for monitoring episodic landslide movements in vegetated terrain. Remote Sens. Environ. 147, 133–144. https://doi.org/10.1016/j.rse.2014.03.003.

Smola, A.J., Schölkopf, B., 2004. A tutorial on support vector regression. Stat. Comput. 14, 199–222. https://doi.org/10.1023/B:STCO.0000035301.49549.88.

Song, J.J., Han, C.J., Li, P., Zhang, J.W., Liu, D.Y., Jiang, M.D., Zheng, L., Zhang, J.K., Song, J.Y., 2012. Quantitative prediction of mining subsidence and its impact on the environment. Int. J. Min. Sci. Technol. 22, 69–73. https://doi.org/10.1016/j.ijmst.2011.07.008.

State Bureau of Coal Industry, 2000. Regulations of Coal Pillar Design and Extraction for Buildings, Water Bodies, Railways, Main Shafts and Roadways. Coal Industry Press, Beijing, China.

Wu, K., 1995. A programme of mining subsidence dynamic prediction and its application. Eng. Surv. Mapp. 4, 44–48. https://doi.org/10.19349/j.cnki.issn1006-7949.1995.03.008.

Wu, K., Ge, J.X., Zhou, M., Yu, F.D., 1998. Some modifications of using probability integral method to predicate model. J. China Coal Soc. 23, 33–36. https://doi.org/10.13225/j.cnki.jccs.1998.01.007.

Yang, Z.F., Li, Z.W., Zhu, J.J., Preusse, A., Hu, J., Feng, G.C., Papst, M., 2018. Time-series 3-D mining-induced large displacement modeling and robust estimation from a single-geometry SAR amplitude data set. IEEE Trans. Geosci. Remote Sens. 56, 3600–3610. https://doi.org/10.1109/TGRS.2018.2802919.

Zebker, H.A., Villasenor, J., 1992. Decorrelation in interferometric radar echoes. IEEE Trans. Geosci. Remote Sens. 30, 950–959. https://doi.org/10.1109/36.175330.

Zhao, C.Y., Lu, Z., Zhang, Q., 2013. Time-series deformation monitoring over mining regions with SAR intensity-based offset measurements. Remote Sens. Lett. 4, 436–445. https://doi.org/10.1080/2150704X.2012.746482.

Zhou, D.W., Wu, K., Cheng, G.L., Li, L., 2015. Mechanism of mining subsidence in coal mining area with thick alluvium soil in China. Arab. J. Geosci. 8, 1855–1867. https://doi.org/10.1007/s12517-014-1382-2.